Inactivation of the murine X-linked juvenile retinoschisis gene, Rs1h, suggests a role of retinoschisin in retinal cell layer organization and synaptic structure

Bernhard H. F. Weber*†, Heinrich Schrewe‡§, Laurie L. Molday¶, Andrea Gehrig*, Karen L. White*, Mathias W. Seeliger‖, Gesine B. Jaissle‖, Christoph Friedburg‖, Ernst Tamm, and Robert S. Molday¶**

*Institute of Human Genetics, Biocenter, University of Würzburg, D-97074 Würzburg, Germany; ‡School of Biosciences, University of Birmingham, Edgbaston, Birmingham B15 2TT, United Kingdom; §Department of Developmental Biology, Max-Planck Institute of Immunobiology, D-79108 Freiburg, Germany; ¶Department of Biochemistry and Molecular Biology and Department of Ophthalmology, University of British Columbia, Vancouver, British Columbia, Canada V6T 1Z4; ‖Retinal Electrodiagnostics Research Group, Department of Pathophysiology of Vision and Neuro-ophthalmology, University of Tübingen, D-72076 Tübingen, Germany; and **Department of Anatomy, University of Erlangen, 91058 Erlangen, Germany

Edited by Jeremy Nathans, Johns Hopkins University School of Medicine, Baltimore, MD, and approved March 12, 2002 (received for review October 5, 2001)

Deleterious mutations in *RS1* encoding retinoschisin are associated with X-linked juvenile retinoschisis (RS), a common form of macular degeneration in males. The disorder is characterized by a negative electroretinogram pattern and by a splitting of the inner retina. To gain further insight into the function of the retinoschisin protein and its role in the cellular pathology of RS, we have generated knockout mice deficient in *Rs1h*, the murine ortholog of the human *RS1* gene. We show that pathologic changes in hemizygous *Rs1h*$^{-/Y}$ male mice are evenly distributed across the retina, apparently contrasting with the macula-dominated features in human. Similar functional anomalies in human and *Rs1h*$^{-/Y}$ mice, however, suggest that both conditions are a disease of the entire retina affecting the organization of the retinal cell layers as well as structural properties of the retinal synapse.

X-linked juvenile retinoschisis (RS) is a common form of macular degeneration in males (1–3). It is characterized by a splitting within the retina at the level of the nerve fiber and ganglion cell layers, resulting in cystic degeneration of the central retina but also may involve the periphery, predominantly the inferotemporal quadrant of the fundus (4–7). Severely affected persons may be blind at birth, although generally the clinical course is more benign, with only a moderate decrease in visual acuity (1). In advanced stages, complications may occur and include vitreal hemorrhages, retinal detachment, and neovascular glaucoma (8). The brief-flash electroretinogram (ERG) of affected males exhibit normal or near normal a-wave amplitudes suggestive of preserved rod and cone photoreceptor systems but substantially reduced b-waves, indicating loss of bipolar cell activity (9).

The gene causing RS was identified by positional cloning (10) and encodes a retina-specific polypeptide of 24 kDa, termed retinoschisin, that is secreted as a disulfide-linked oligomeric protein complex from both the rod and cone photoreceptors and the bipolar cells (11, 12). The protein consists almost exclusively of a discoidin-like domain first characterized in the *Dictyostelium discoideum* protein discoidin I (ref. 13). Discoidin domains are found in a large family of secreted or membrane-bound proteins and have been implicated in cell adhesion and cell–cell interaction (14, 15).

To gain further insight into the function of retinoschisin and its role in the cellular pathology of RS, we have generated knockout mice deficient in *Rs1h*, the murine ortholog of *RS1* (ref. 16). Histologically, we found a marked splitting of the inner nuclear layer, overall disorganization of the retinal cell layers with irregular displacement of cells, and later degeneration of the photoreceptors that appears more pronounced in cones. These findings are supported by *in vivo* imaging, electrodiagnostic data, immunolabeling studies, and transmission electron microscopy. In the *Rs1h*$^{-/Y}$ retina, we observed disturbed vectorial transport of MAGUK protein PSD-95 to the outer and inner plexiform layers, where the X-linked juvenile retinoschisis-1 (Rs1h) protein is ordinarily present in high amounts. Our findings suggest that, via its discoidin domain, retinoschisin may directly or indirectly be involved in retinal cell-layer architecture and synaptic structure.

Methods

Construction of the Rs1h Gene-Targeting Vector. Parts of the 5′ (intron 2 to exon 3) and 3′ (exon 4 to intron 5) genomic regions of the murine *Rs1h* gene were amplified from CJ7 embryonic stem (ES) cell DNA (17) with PCR primers rsmint2FGGG (5′-GGG AGT CGA CTG AGT GGA AAG GCA GGT CT-3′)/rsm3R (5′-TGG AAT ACA GTC TAA GGA GG-3′) and rsm4F (5′-CCA ACC CAG AGC AGT ATG TG-3′)/rsm6R (5′-GAT GAA GCG GGA AAT GAT GG-3′), respectively. The *lacZ* gene was cloned in-frame into exon 3 as part of a bpA-*PGK-neo*^{r}-bpA cassette, resulting in a final targeting construct in which the cassette is flanked by the 5′ (2.4 kb) and 3′ (3.5 kb) sequences homologous to the wild-type (wt) allele (Fig. 1*a*). Thereby, parts of exons 3 and 4, as well as the entire intron 3, were deleted in the targeting construct. Before electroporation, the resulting plasmid was linearized with *Sma*I.

Generation of Rs1h-Deficient Mice. CJ7 ES cells were electroporated and selected as described (17). DNA was isolated from 300 colonies according to published methods (18). Positive homologous recombination was identified by Southern blot analysis by using 5′ and 3′ probes external to the targeting construct generated with primer pairs rsm2F (5′-CAC ATT GGG ATT GTC ATC G-3′)/rsmint2R (5′-GGC TTC AGG AGT AGG GTA TC-3′) and rsm3′pF (5′-TGT AGC AAC CAT CCA ATA GG-3′)/rsm3′pR (5′-ATG TCC TCG TAT GTG CTA AG-3′), respectively, as well as by PCR with primer pairs rsm2F/lacZR2

Abbreviations: RS, X-linked juvenile retinoschisis; ERG, electroretinography; ES, embryonic stem; wt, wild type; POS, photoreceptor outer segments; Rs1h, X-linked juvenile retinoschisis-1, homologue; SLO, scanning-laser ophthalmoscopy; INL, inner nuclear layer; IPL, inner plexiform layer; OPL, outer plexiform layer.

†To whom reprint requests should be addressed at: Institute of Human Genetics, Biocenter, Am Hubland, D-97074 Würzburg, Germany. E-mail: bweb@biozentrum.uni-wuerzburg.de.

The publication costs of this article were defrayed in part by page charge payment. This article must therefore be hereby marked "*advertisement*" in accordance with 18 U.S.C. §1734 solely to indicate this fact.

 www.pnas.org/cgi/doi/10.1073/pnas.092528599

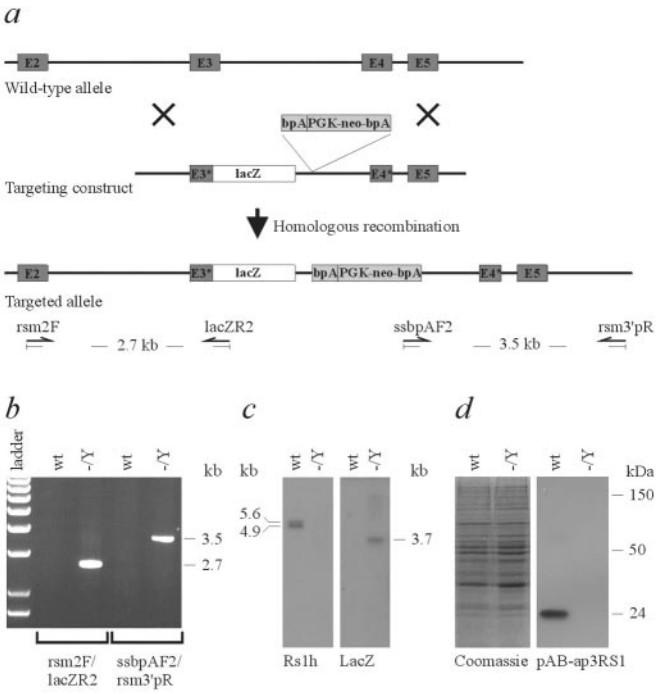

Fig. 1. Targeted disruption of exon 3 of the *Rs1h* gene. (*a*) In the targeting construct, 1 bp of exon 3 (E3*), all of intron 3, and 66 bp of exon 4 (E4*) are deleted and replaced with a *lacZ-neo*^{r} cassette. (*b*) PCR amplification demonstrates the correct targeting of *Rs1h*. The relative positions of oligonucleotide primers and expected product sizes are given in *a*. (*c*) By using a probe spanning exons 4 to 6 of *Rs1h*, Northern blot analyses reveal the expected 5.6- and 4.9-kb transcripts in eye total RNA from the wt (wt) but not from the *Rs1h* knockout (−/Y) male mouse. Subsequent hybridization with a *lacZ* probe exhibits a fusion transcript of 3.7 kb only in the Rs1h-deficient animal. (*d*) Western blot analysis using eye cup protein extracts. Polyclonal antibody pAB-ap3RS1 labels the 24-kDa RS1 protein in WT mice. With the same antibody, the expected fusion protein of 120 kDa is not observed in mutant males, although it contains the antibody epitope, thus indicating that the targeted allele represents a true null allele. Equal loading of protein extracts is demonstrated by Coomassie staining.

(5′-CAA GGC GAT TAA GTT GGG TAA C-3′) and ssbpAF2 (5′-AGA GCT CCG CGG CTC GAC TGT GCC TTC TAG TT-3′)/rsm3′pR (Fig. 1 *a* and *b*). The injection of mutant ES cells into C57BL/6 blastocysts (19) resulted in five high-percentage coat-color chimeras, two of which exhibited germline transmission when bred to C57BL/6 females. Female F1 animals heterozygous for the *Rs1h* mutation were intercrossed with C57BL/6 mice to generate hemizygous male offspring.

Northern Blot Analysis. Total RNA from murine eye cups was prepared by using standard techniques. Hybridization probes were generated by RT-PCR, with primers rsm4F/rsm6R encompassing exons 4 to 6 of the *Rs1h* gene and by excision of the recombinant *lacZ* gene. The fragments were randomly labeled in the presence of ^{32}PdCTP (3,000 Ci/mmol; 1 Ci = 37 GBq).

Western Blot Analysis. Polyclonal peptide antibody pAB-ap3RS1 (ref. 12) was affinity purified from rabbit antiserum. Peroxidase-conjugated anti-rabbit IgG was used as a secondary antibody and visualized by using the enhanced chemiluminescence detection system (Amersham Pharmacia).

Scanning-Laser Ophthalmoscopy. Fundus imaging was performed with an HRA scanning-laser ophthalmoscope (SLO) with an infrared wavelength of 835 nm (Heidelberg Instruments, Heidelberg, Germany). The confocal diaphragm of the SLO allows imaging of different planes of the posterior pole, ranging from the surface of the retina down to the retinal pigment epithelium (RPE) and the choroid. Different planes can be viewed sequentially by varying the focus by about ±20 diopters.

Electroretinogram. ERGs were obtained according to reported procedures (20). Briefly, before anesthesia with ketamine (66.7 mg/kg), xylazine (11.7 mg/kg), and atropine (1 mg/kg), the pupils of dark-adapted mice were dilated. The ERG equipment consisted of a Ganzfeld bowl, a DC amplifier, and a PC-based control and recording unit (Toennies Multiliner Vision, Hoechberg, Germany). Band-pass filter cut-off frequencies were 0.1 and 3,000 Hz. Single flash recordings were obtained both under dark-adapted (scotopic) and light-adapted (photopic) conditions. Light adaptation before the photopic session was performed with a background illumination of 30 cd/m^2 for 10 min. Single flash stimulus intensities were increased from 10^{-4} cd·s/m^2 to 25 cd·s/m^2 and divided into 10 steps of 0.5 and 1 log cd·s/m^2. Ten responses were averaged, with an inter-stimulus interval of either 5 s or 17 s (for 1, 3, 10, 25 cd·s/m^2).

Histology and Electron Microscopy. Two-month-old mutant mice and wt littermates were perfusion-fixed via the heart with Ito's fixative (21). After enucleation, the eyes were bisected equatorially and immersed in the same fixative for 24 h. After fixation, the samples were washed overnight in cacodylate buffer, post-fixed with OsO_4, dehydrated, and embedded in Epon (Fa. Roth, Karlsruhe, Germany). Semithin sections (1 μm) were stained with toluidine blue for serial histological analysis. Ultrathin sections were stained with uranyl acetate and lead citrate and viewed with an EM 902 electron microscope (Zeiss).

Immunofluorescence Labeling. For immunofluorescence studies, retina dissected from two-month-old mutant and wt mice were paraformaldehyde-fixed for 1–2 h and subsequently rinsed in PBS containing 10% (wt/vol) sucrose. Cryosections were blocked with PBS containing 0.2% Triton X-100 (PBS-T) and 10% (vol/vol) goat serum for 20 min and labeled overnight with the primary antibody. The samples then were rinsed in PBS and labeled for 1 h with the secondary antibody conjugated to Cy3 (red) or Alexi 488 (green) (Jackson ImmunoResearch). The Rs1 3R10 monoclonal antibody was produced from a mouse immunized with a glutathione *S*-transferase fusion protein containing the LSSTEDEGEDPWYQKAC peptide, corresponding to amino acids 22–39 of the human RS1 precursor protein (10). Cell-specific antibodies used were Rho 1D4 monoclonal antibody to rhodopsin (22), Mab 115A10 monoclonal antibody to rat olfactory bulb (a generous gift of Shinobu C. Fujita, Mitsubishi Kasei Institute of Life Sciences, Tokyo; ref. 23); JH 492 polyclonal antibody to red/green (middle wavelength) cone opsin and JH 455 blue (short wavelength) cone opsin (a generous gift of J. Nathans, Johns Hopkins University, Baltimore), PAN-SAP polyclonal antibody (a generous gift of Craig C. Garner, Department of Neurobiology, Univ. of Alabama, Birmingham) and 7E3–1B8 monoclonal antibody (Affinity BioReagents, Golden, CO) to the postsynaptic density protein 95 (PSD95), and CRALBP polyclonal antibody to cellular retinal binding protein (a generous gift of Jack Saari, Department of Ophthalmology, Univ. of Washington, Seattle; ref. 24). The PAN-SAP and 7E3–1B8 antibodies showed the same labeling pattern, although the PAN-SAP stained mouse retina more intensely.

Cone Photoreceptor Count. The relative number of cone photoreceptor cells was estimated from counts of total cone opsin-labeled cells (JH492 and JH455) in a series of retinal sections through the eyes of three wt and *Rs1h*$^{-/Y}$ mice, respectively.

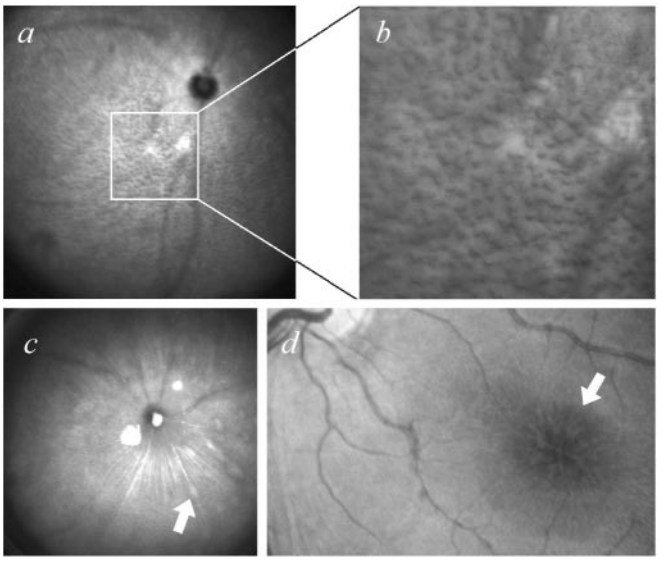

Fig. 2. Macromorphological evaluation of the *Rs1h*$^{-/Y}$ retina with scanning laser ophthalmoscopy. (*a*) Survey of the fundus, demonstrating a layer of cyst-like elevations in the inner retina. (*b*) Optical magnification reveals that the densely packed structures are clearly demarcated from the surrounding normal-appearing regions. (*c*) Focus on the retinal surface shows superficial vessels and the nerve fiber layer. Visible in the lower right quadrant are several larger cysts, one displacing a retinal vessel (arrow). (*d*) Fundus photograph of a patient with RS, featuring typical small macular cysts arranged in a stellate pattern (arrow) and radial striae centered on the fovea. There is an obvious similarity to the appearance of the mouse retina as shown in *b*.

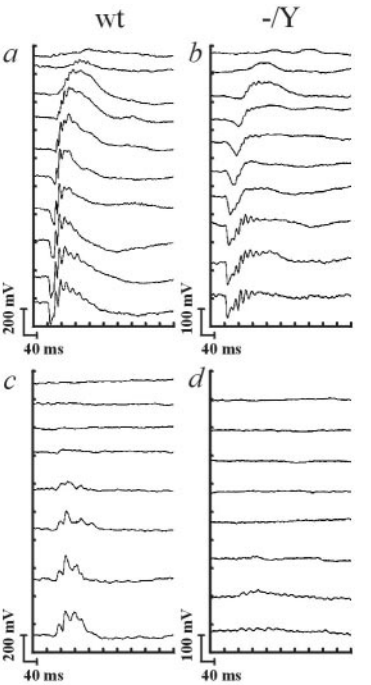

Fig. 3. Electrophysiology of Rs1h$^{-/Y}$ and wt mice. Scotopic intensity series of a wt (*a*) and an Rs1h mutant mouse (*b*). Log light intensities (from top to bottom) were −4, −3, −2, −1.5, −1, −0.5, 0, 0.5, 1, 1.5 log cd·s/m^2. The overall loss of amplitude and the additional selective reduction of the b-wave are clearly visible. Photopic intensity series of a wt control (*c*) and an Rs1h-deficient mouse (*d*). Log light intensities (from top to bottom) were −2, −1.5, −1, −0.5, 0, 0.5, 1, 1.5 log cd·s/m^2. The photopic ERG of the Rs1h$^{-/Y}$ mice is strongly reduced, indicating a much more severe cone than rod dysfunction.

Results

Disruption of the *Rs1h* gene was obtained by introducing a *lacZ* reporter gene in-frame into exon 3 of the *Rs1h* gene together with a neomycin-resistance gene (*neo*) expression cassette under the separate control of the mouse phosphoglycerate kinase gene (*Pgk*) promoter (Fig. 1*a*). Successful germline transmission of the correctly targeted allele was confirmed in the F1 generation by PCR analysis of tail DNA with primers rsm2F/lacZR2 and ssbpAF2/rsm3′pR (Fig. 1 *a* and *b*). Carrier female offspring (*Rs1h*$^{-/+}$) were mated with C57BL/6 male mice to obtain hemizygous *Rs1h*$^{-/Y}$ males whose general appearance was indistinguishable from their wt litter mates. Northern blot analysis of eye cup RNA from 6-week-old mice with an *Rs1h*3′-UTR probe detects 5.6- and 4.9-kb transcripts in wt but not in *Rs1h*$^{-/Y}$ mice, whereas a *lacZ* probe reveals the expected 3.7-kb fusion transcript in the mutant animals (Fig. 1*c*). However, the translation product of the fusion transcript was not detected by Western blot analysis with the pAB-ap3RS1 antibody directed against the N terminus of human retinoschisin (12), indicating that the disrupted *Rs1h* locus represents a true null allele (Fig. 1*d*).

In vivo imaging of 3-month-old *Rs1h*$^{-/Y}$ mice with an SLO revealed a densely packed layer of small cyst-like structures in the inner retina, sometimes extending to the nerve fiber layer (Fig. 2 *a* and *b*). In contrast to the human condition where the cyst formation is largely restricted to the macular area (Fig. 2*d*), their distribution was homogenous across the entire retina (Fig. 2 *a* and *b*). Similar to human, larger cysts were observed in the retinal periphery of *Rs1h*$^{-/Y}$, which, in some instances, displaced superficial retinal vessels (Fig. 2*c*).

Analogous to the "negative ERG" typically observed in human RS (1, 25), dark-adapted (scotopic) ERGs in the *Rs1h*$^{-/Y}$ mice showed a dramatic loss of the positive b-wave, which is mostly shaped by the neurons of the inner retina. Although amplitudes were less than one-half of normal, the negative a-wave representing both inner and outer retinal components was relatively preserved (Fig. 3 *a* and *b*). Under light-adapted (photopic) conditions, ERG responses were virtually absent, suggesting a profound dysfunction of the cone system (Fig. 3 *c* and *d*). A more specific analysis of rod photoreceptor responses using the double flash method (26) did not show detectable abnormalities beyond amplitude reduction (data not shown), indicating that *Rs1h* deficiency does not specifically impair rod function. Taken together, the ERG findings suggest a decrease in the number of functional photoreceptors with the remaining cells responding normally to light stimuli. The additional selective attenuation of the b-wave, in conjunction with the retinal depth estimate of the cyst layer by SLO and previous evidence that retinoschisin is associated with photoreceptors and bipolar cells (12), point to the bipolar cell layer or the bipolar cell/photoreceptor connection as likely sites of pathology in *Rs1h*$^{-/Y}$ mice.

Histologic examination of retina sections from two-month-old wt and *Rs1h*$^{-/Y}$ mice showed striking changes in the inner and outer nuclear layers (INL and ONL) of the mutant animals. Essentially, a pronounced disorganization of the retinal layers was observed, accompanied by a significant reduction in the number of photoreceptor nuclei (Fig. 4 *a–c*). In two Rs1h$^{-/Y}$ eyes, areas with preserved photoreceptor outer segments (POS) were still present at this age (Fig. 4*b*), whereas one mutant animal revealed an almost complete absence of POS over the entire retinal sections (Fig. 4*c*), suggesting a certain degree of heterogeneity in disease phenotype. Mainly in those areas where photoreceptor outer segments were still present, large schisis-like gaps were observed between the cells of the inner nuclear layer (Fig. 4*b*). In areas of Rs1h$^{-/Y}$ retinae where complete loss

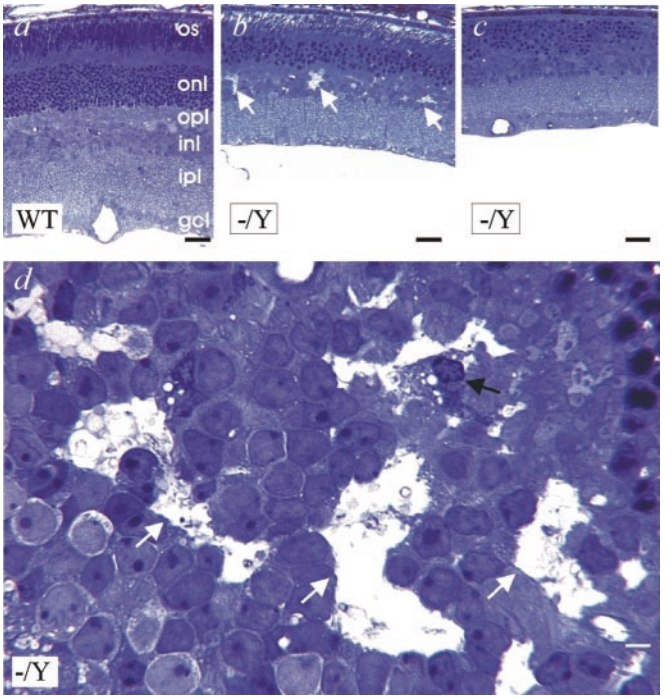

Fig. 4. (*a–d*) Semithin retinal sections of wt (WT) and Rs1h$^{-/Y}$ (−/Y) mice at 2 months of age. In meridional sections, the thickness of the central retina is markedly reduced in Rs1h$^{-/Y}$ mice (*b* and *c*) as compared with wt mice (*a*). In some Rs1h$^{-/Y}$ eyes, photoreceptor outer segments (POS) are present (*b*), whereas others show partial or complete absence of the POS (*c*). In Rs1h$^{-/Y}$ eyes with areas of preserved POS, large gaps are present between the cells of the INL (arrows in *b*). Such gaps are absent in areas with complete degeneration of POS (*c*). (*d*) Oblique tangential section through the INL of an Rs1h$^{-/Y}$ retina reveals large extracellular gaps (white arrows). In some of the gaps, cell bodies of microglia are observed (black arrow). os, photoreceptor outer segments; onl, outer nuclear layer; opl, outer plexiform layer, inl, inner nuclear layer; ipl, inner plexiform layer; gcl, ganglion cell layer. [Bars = 25 μm (*a–c*) and 2.8 μm (*d*).]

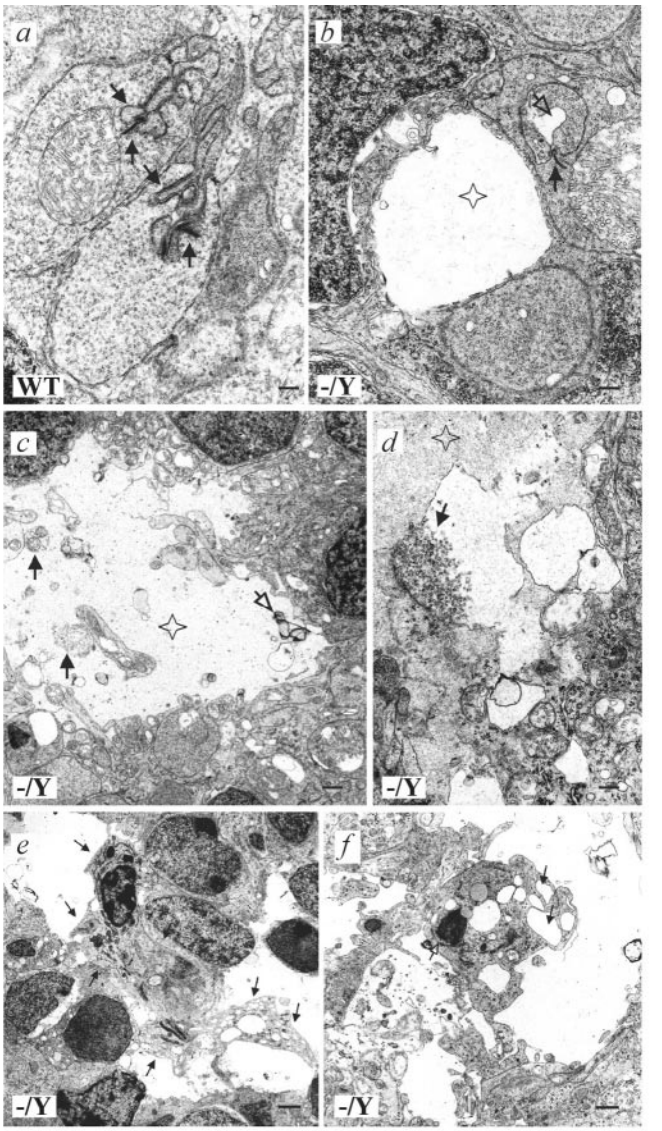

Fig. 5. (*a–f*) Electron microscopy of the retina of wt (WT) and Rs1h$^{-/Y}$ (−/Y) mice at 2 months of age. (*a*) In the retina of wt mice, typical ribbon synapses are present at the photoreceptor terminals (black arrows). (*b*) In the retina of Rs1h$^{-/Y}$ mice, increased extracellular spaces (open arrow) are observed in regions of ribbon synapses (solid arrow). Larger extracellular gaps are present between individual photoreceptor terminals (asterisk). (*c*) The extracellular gaps (asterisk) in the INL of Rs1h$^{-/Y}$ mice are filled with cellular debris (solid arrows) and membranous whorls (open arrow). (*d*) Part of the extracellular debris in the INL gaps (asterisk) of Rs1h$^{-/Y}$ mice consists of fragmented nerve cell terminals (solid arrow) containing synaptic vesicles. (*e*) Cells with ultrastructural characteristics of microglia in the retina of Rs1h$^{-/Y}$ mice. In the increased extracellular spaces, cells with long cytoplasmic processes (arrows) are observed. (*f*) Upon higher magnification, multiple clear vesicles (solid arrow) and electron-dense phagolysosomes (open arrow) are observed in the cytoplasm of the cells. [Bars = 0.53 μm (*a*, *b*, *d*, and *f*) and 1.4 μm (*c* and *e*).]

of photoreceptor outer segments was obvious, schisis formation was not evident histologically (Fig. 4*c*).

Normal ribbon synapses were found by electron microscopy at the photoreceptor terminals of a two-month-old wt mouse (Fig. 5*a*). In contrast, the retina of an Rs1h$^{-/Y}$ littermate revealed increased extracellular spaces in the region of photoreceptor ribbon synapses. In addition, larger extracellular gaps were present between individual photoreceptor terminals (Fig. 5*b*) and the perikarya of the inner nuclear layer (Fig. 5*c*). The extracellular gaps (asterisk in Fig. 5*c*) in the inner nuclear layer of the Rs1h$^{-/Y}$ retina were filled with membranous whorls and cellular debris containing fragmented mitochondria and nerve-cell terminals (Fig. 5 *c* and *d*). In addition, cells with ultrastructural characteristics of microglia, which expressed long cytoplasmic processes, multiple clear vesicles, and electron-dense phagolysosomes were present in the spaces (Fig. 5 *e* and *f*).

To delineate further the consequences of Rs1h deficiency for specific retinal cell types, cryosections from wt and *Rs1h*$^{-/Y}$ retinas were labeled with cell-specific antibodies for analysis by immunofluorescence microscopy (Fig. 6 *a–l*). Supporting our Western blot results (Fig. 1*d*), Rs1 3R10 antibody labeling was absent from the mutant retina (Fig. 6*a*). DAPI staining identifies some nuclei (cells) past the outer limiting membrane and in the inner and outer segment layers as well as displacement of nuclei into the inner plexiform layer (IPL; Fig. 6*a*). The wt retina shows a typical distribution of Rs1h with the protein localizing throughout much of the inner and outer retina with intense staining of the photoreceptor inner segments and bipolar cells (Fig. 6*b*; ref. 12). In addition, significant amounts of Rs1h are present in the IPL and outer plexiform layer (OPL). Immunolabeling of rhodopsin shows that it is translocated to the outer segments in the *Rs1h*$^{-/Y}$ mouse, although the outer segments appear disorganized compared with those in wt retina (Fig. 6 *c* and *d*). Analysis of short and medium cone opsin-immunolabeled cells indicated that there were three times fewer cones in the retina of *Rs1h*$^{-/Y}$ mice than in wt mice. A marked delocalization of opsin to the

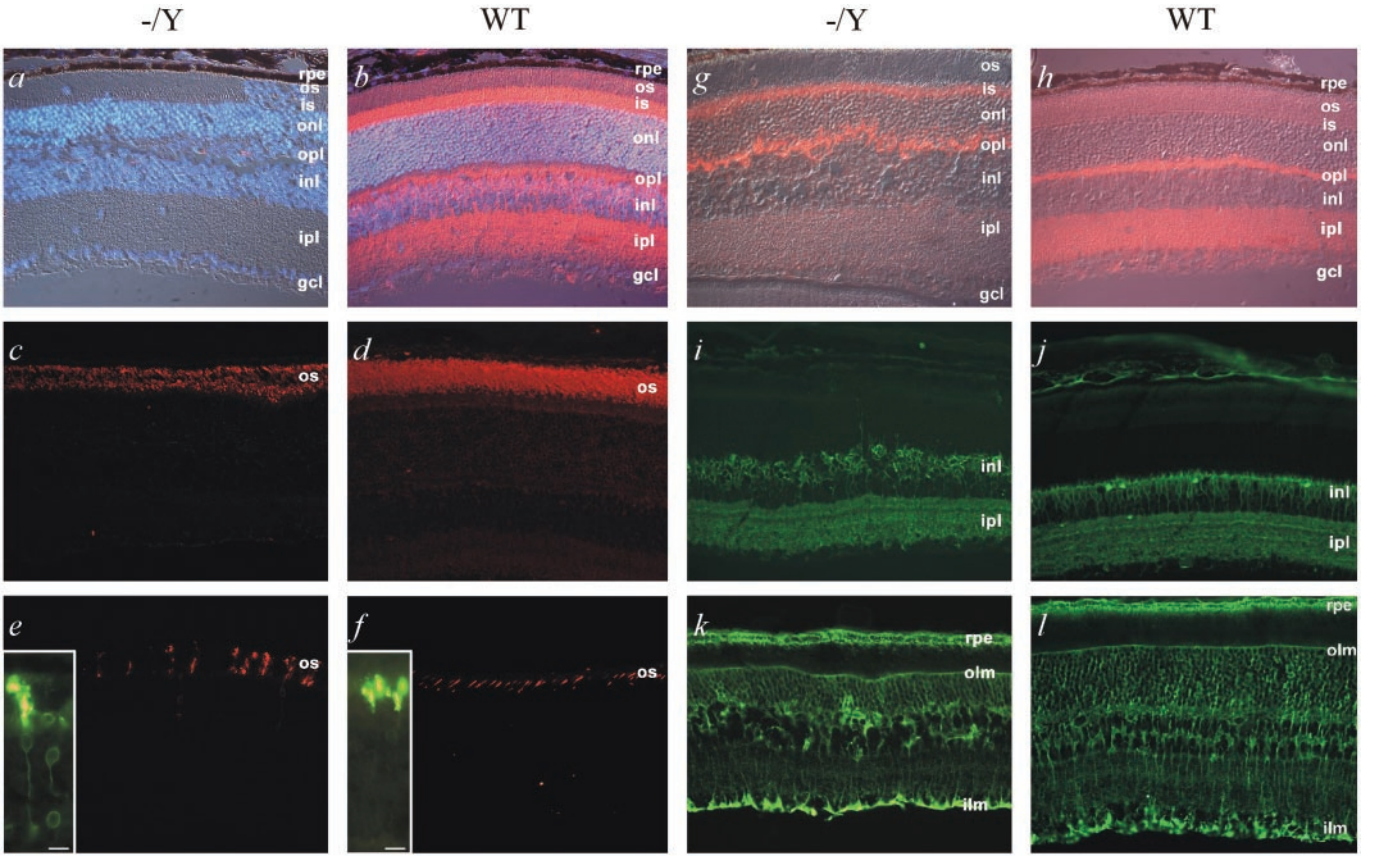

Fig. 6. Immunofluorescence microscopy of retinal cryosections from 2-month-old *Rs1h*$^{-/Y}$ and wt mice. (*a* and *b*) Rs1 labeling with the Rs1 3R10 monoclonal antibody (red). Image is merged with DAPI nuclear staining (blue) and differential interference contrast (DIC) microscopy. (*c* and *d*) Rhodopsin staining with the Rho 1D4 monoclonal antibody. (*e* and *f*) Cone opsin labeling with a mixture of polyclonal antibody JH 455 and JH 492. (*Insets*) Bar = 10 μm. (*g* and *h*) PAN-SAP antibody labeling of PSD-95 in the OPL and IPL in the wt mouse compared with the IS and OPL in the *Rs1h*$^{-/Y}$ mouse. Image is merged with DIC image showing the retinal layers. (*i* and *j*) Labeling of bipolar cells with the monoclonal antibody Mab 115A10. (*k* and *l*) Labeling of Mueller cells and retinal pigment epithelial (RPE) cells with an anti-CRALBP antibody. Abbreviations used are as in Fig. 4, plus (is), inner segment.

inner segment, cell body, and synaptic region was evident in many cone photoreceptors of the Rs1h$^{-/Y}$ knockout, but not wt, mice (Fig. 6 *e*, *f*, and *Insets*). Labeling of the postsynaptic density (PSD)-95 MAGUK protein with the PAN-SAP or 7E3–1B8 antibody produces immunoreactivity in the OPL and IPL of the retina of the wt mouse (Fig. 6*h*), similar to that described for rat retina (27). In the *Rs1h*$^{-/Y}$ retina, the staining pattern reveals significant disorganization of the OPL and an accumulation of PSD-95 in the photoreceptor inner segment (Fig. 6*g*). In addition, there is a significant decrease in PSD-95 in the IPL (Fig. 6*g*). By using monoclonal antibody Mab 115A10, substantial disorganization also is evident that involves the INL bipolar cells of the mutant retina (Fig. 6 *i* and *j*). Staining of the Mueller cells with an anti-CRALBP antibody shows a similar pattern in both knockout and wt mice; however, in the mutant retina, areas devoid of staining within the INL and more intense staining of the inner limiting membrane were observed (Fig. 6 *k* and *l*).

Discussion

In this report, we present the generation and characterization of an *Rs1h*$^{-/Y}$ knockout mouse. It establishes this mouse line as a valuable model for RS with a retinal phenotype closely paralleling that of the human condition. Although the murine retina lacks a macular organization, our findings in the *Rs1h*$^{-/Y}$ mutant animals demonstrate that mice can still be useful for modeling human diseases that display a primary macular phenotype such as RS.

The major pathology in the retina of the retinoschisin-deficient mouse seems to be a generalized disruption of cell layer architecture, most evident in the loss of integrity of the OPL/INL and an irregular displacement of cells in various retinal layers. Functionally, ERG recordings point to severe impairment of bipolar cell-associated pathways and a loss of photoreceptors that is more pronounced in cone than in rod pathways. This finding also is supported by immunofluorescence labeling studies. Rod staining indicates a generalized decrease in cell number, whereas cone labeling demonstrates a more striking cell loss as well as a defect in the targeting of cone opsin to the outer segments. Similarly, in the organization of the bipolar cell layer, there are clear abnormalities, which may be instrumental to the relative b-wave attenuation demonstrated by ERG recordings in human (28, 29) and the *Rs1h*$^{-/Y}$ mouse.

The observed distortion of retinal layers in the *Rs1h*$^{-/Y}$ mouse could be explained by the loss of cell–cell and/or cell–matrix interactions, both of which are thought to be mediated by the discoidin domain of retinoschisin (14, 15). The functional importance of this domain also is reflected by the mutational profile determined in more than 320 RS patients worldwide (http://www.dmd.nl/rs/rshome.html). Of the 125 distinct sequence changes identified so far, 101 (81%) occur in exons 4 to 6 that encode the discoidin motif and likely impair defined functional aspects of this domain. Two types of discoidin-mediated binding can be envisioned. A collagen–discoidin interaction (30, 31) could anchor cells into an extracellular matrix

scaffold or mediate transmembrane-signaling processes. For example, in a direct ligand-binding assay, the introduction of amino acid mutations in the discoidin domain of the discoidin domain receptor 1 (DDR1) at positions homologous to several retinoschisin mutations affects collagen binding and/or receptor phosphorylation of DDR1 (ref. 32). These experiments suggest that binding of discoidin domains to (collagenous) components of the extracellular matrix could be a more general property of these modules. Binding to membrane-anchored carbohydrate residues could represent an alternative mode of discoidin-mediated function. Such interactions would facilitate cell-to-cell contacts and are thought to play a critical role in the activation of the blood clotting cascade on platelet membrane surfaces (33, 34).

One of the most important cellular contacts in the retina occurs at the synapse, where retinoschisin is ordinarily present in high amounts (Fig. 6*b* and ref. 12). Our finding of loss of the synaptic MAGUK protein PSD-95 in the IPL of the *Rs1h* deficient mouse and defects in its translocation to the OPL points to a direct or indirect role of retinoschisin in the proper assembly and stabilization of this region of the cell. This finding also is supported by transmission electron microscopy revealing atypical ribbon synapse formation at the photoreceptor terminals of $Rs1h^{-/Y}$ mice. Failure to establish or maintain the proper synaptic connections could lead to subsequent photoreceptor cell death, a phenomenon that also has been reported in an animal model transgenic for P347L rhodopsin (35).

Earlier studies have suggested that the Müller cells are primarily involved in RS1 pathology (6, 7), a view that has recently been challenged by the fact that retinoschisin was not detected on Müller glial cells (12). In agreement with the latter findings, the Müller cells seem to be relatively unaffected in the $Rs1h^{-/Y}$ retina, arguing for a secondary rather than a primary role of these glial cells in the disease process. A more detailed analysis of cytoplasmic and membranous Müller cell proteins will be required to address the extent of involvement of this particular cell type in disease evolution.

The $Rs1h^{-/Y}$ mouse shares several diagnostic features with human RS, including the typical ''negative ERG'' response and the development of cystic structures within the inner retina, followed by a dramatic loss of photoreceptor cells. Therefore, we conclude that the $Rs1h^{-/Y}$ mouse represents an important model system for further investigations into the molecular mechanisms underlying the cellular disorganization of the retinal structure. This model may be particularly useful to evaluate the role of retinoschisin in the assembly and stabilization of synaptic contacts and will provide a suitable experimental system for novel therapeutic approaches in X-linked juvenile retinoschisis.

We thank Benoît Kanzler for ES cell injection, Vladimir Milenkovic for assistance with the Western blot experiment, and Andrea Rivera for help with mouse breeding. This work was supported by Deutsche Forschungsgemeinschaft Grants We1259/12-2, Se837/1-1, and SFB 430 C2 and National Eye Institute Grant EY 2422.

1. Kellner, U., Brummer, S., Foerster, M. H. & Wessing, A. (1990) *Arch. Clin. Exp. Ophthalmol.* **228,** 432–437.
2. George, N. D., Yates, J. R. & Moore, A. T. (1995) *Br. J. Ophthalmol.* **79,** 697–702.
3. Puech, B., Kostrubiec, B., Hache, J. C. & Francois, P. (1991) *J. Fr. Ophtalmol.* **4,** 153–164.
4. Yanoff, M., Kertesz-Rahn, E. & Zimmerman, L. E. (1968) *Arch. Ophthalmol.* **79,** 49–53.
5. Manschot, W. A. (1972) *Arch. Ophthalmol.* **88,** 131–138.
6. Condon, G. P., Brownstein, S., Wang, N. S., Kearns, J. A. & Ewing, C. C. (1986) *Arch. Ophthalmol.* **104,** 576–583.
7. Kirsch, L. S., Brownstein, S. & de Wolff-Rouendaal, D. (1996) *Can. J. Ophthalmol.* **31,** 301–310.
8. Roesch, M. T., Ewing, C. C., Gibson, A. E. & Weber, B. H. F. (1998) *Can. J. Ophthalmol.* **33,** 149–158.
9. Robson, J. G. & Frishman, L. J. (1998) *Doc. Ophthalmol.* **95,** 187–215.
10. Sauer, C. G., Gehrig, A., Warneke-Wittstock, R., Marquardt, A., Ewing, C. C., Gibson, A., Lorenz, B., Jurklies, B. & Weber, B. H. F. (1997) *Nat. Genet.* **17,** 164–170.
11. Reid, S. N., Akhmedov, N. B., Piriev, N. I., Kozak, C. A., Danciger, M. & Farber, D. B. (1999) *Gene* **227,** 257–266.
12. Molday, L. L., Hicks, D., Sauer, C. G., Weber, B. H. F. & Molday, R. S. (2001) *Invest. Ophthalmol. Visual Sci.* **42,** 816–825.
13. Simpson, D. L., Rosen, S. D. & Barondes, S. H. (1974) *Biochemistry* **13,** 3487–3493.
14. Baumgartner, S., Hofmann, K., Chiquet-Ehrismann, R. & Bucher, P. (1998) *Protein Sci.* **7,** 1626–1631.
15. Vogel, W. (1999) *FASEB J.* **13,** S77–S82.
16. Gehrig, A. E., Warneke-Wittstock, R., Sauer, C. G. & Weber, B. H. F. (1999) *Mamm. Genome* **10,** 303–307.
17. Swiatek, P. J. & Gridley, T. (1993) *Genes Dev.* **7,** 2071–2084.
18. Ramirez-Solis, R., Davis, A. C. & Bradley, A. (1993) *Methods Enzymol.* **225,** 855–878.
19. Schrewe, H., Gendron-Maguire, M., Harbison, M. L. & Gridley, T. (1994) *Mech. Dev.* **47,** 43–51.
20. Seeliger, M. W., Grimm, C., Stahlberg, F., Friedburg, C., Jaissle, G., Zrenner, E., Guo, H., Reme, C. E., Humphries, P., Hofmann, F., *et al.* (2001) *Nat. Genet.* **29,** 70–74.
21. Ito, S. & Karnovsky, M. J. (1968) *J. Cell Biol.* **39,** 168A–169A.
22. MacKenzie, D. & Molday, R. S. (1982) *J. Biol. Chem.* **157,** 7100–7105.
23. Onoda, N. & Fujita, S. C. (1987) *Brain Res.* **416,** 359–363.
24. Bunt-Milam, A. H. & Saari, J. C. (1983) *J. Cell Biol.* **97,** 703–712.
25. Hirose, T., Wolf, E. & Hara, A. (1977) *Doc. Ophthalmol. Proc. Ser.* **13,** 173–184.
26. Hetling, J. R. & Pepperberg, D. R. (1999) *J. Physiol.* **516,** 593–609.
27. Koulen, P., Fletcher, E. L., Craven, S. E., Bredt, D. S. & Wässle, H. (1998) *J. Neurosci.* **18,** 10136–10149.
28. Green, D. G. & Kapousta-Bruneau, N. V. (1999) *Visual Neurosci.* **16,** 727–741.
29. Lei, B. & Perlman, I. (1999) *Visual Neurosci.* **16,** 743–754.
30. Shrivastava, A., Radziejewski, C., Campbell, E., Kovac, L., McGlynn, M., Ryan, T. E., Davis, S., Goldfarb, M. P., Glass, D. J., Lemke, G. & Yancopoulos, G. D. (1997) *Mol. Cell* **1,** 25–34.
31. Vogel, W., Gish, G. D., Alves, F. & Pawson, T. (1997) *Mol. Cell* **1,** 13–23.
32. Curat, C. A., Eck, M., Dervillez, X. & Vogel, W. F. (2001) *J. Biol. Chem.* **276,** 45952–45958.
33. Kim, S. W. Quinn-Allen, M. A., Camp, J. T., Macedo-Ribeiro, S., Fuentes-Prior, P., Bode, W. & Kane, W. H. (2000) *Biochemistry* **39,** 1951–1958.
34. Knight, C. G., Morton, L. F., Onley, D. J., Peachey, A. R., Ichinohe, T., Okuma, M., Farndale, R. W. & Barnes, M. J. (1999) *Cardiovasc. Res.* **41,** 450–457.
35. Blackmon, S. M., Peng, Y. W., Hao, Y., Moon, S. J., Oliveira, L. B., Tatebayashi, M., Petters, R. M. & Wong, F. (2000) *Brain Res.* **885,** 53–61.